Table DR1: Sample locations and AFT data.

Sample	Stratigraphic age ± error [Ma]	Latitude	Longitude	Elevation [m]	# grains	ρs	Ns	ρi	Ni	ρd	Nd	P(χ²) [%]	Dispersion	age range [Ma]	U [ppm]
CGP100a	3.5±1.0	45.29066	5.07053	360	100	3.198	1566	24.617	12053	8.858	4511	0	0.28	4.9-37.1	41±20
CGP101	4.2±0.5	45.29326	5.06389	330	100	5.375	2635	32.178	15774	8.863	4511	0	0.46	6.6-228	56±32
CGP103	3.2±1.0	45.28458	5.05568	377	100	3.446	1933	27.957	15682	8.868	4511	0	0.28	3.3-32.0	46±24
CGP104	2.5±1.0	45.28474	5.05718	406	100	3.394	1602	26.423	12473	8.874	4511	0	0.27	3.8-37.7	47±26
CGP106	13.0±2.0	45.26658	5.04739	353	100	2.838	1639	21.601	12475	8.879	4511	0	0.22	7.1-51.2	37±25
CGP107	5.0±0.3	45.20684	5.02350	330	100	3.732	1950	25.479	13312	8.843	4511	0	0.24	5.7-34.1	44±28
CGP108	17.5±2.0	45.30943	5.64158	425	92	6.106	1944	19.139	6093	8.900	4511	0	0.80	9.2-1275	32±23
CGP109	11.5±0.5	45.27043	5.34524	538	100	4.969	3313	20.082	13388	8.895	4511	0	0.91	7.6-230	34±24
CGP110a	10.0±2.0	45.28296	5.34196	669	100	5.128	2623	26.774	13695	8.901	4511	0	0.25	10.6-54.9	49±32
CGP111	13.0±2.0	45.20294	5.21103	482	100	5.162	2270	28.583	12570	8.911	4511	17	0.09	6.6-39.5	51±29
CGP112a	5.5±0.5	45.01260	4.93544	174	100	5.546	2826	19.289	9828	8.917	4511	0	0.95	6.5-305	41±42
CGP113a	15.0±1.0	45.01310	4.93475	153	99	5.044	2530	17.006	8530	8.922	4511	0	0.87	6.1-261	28±18
CGP114	15.0±1.0	45.01295	4.93473	145	100	3.421	2083	15.593	9493	8.933	4511	0	0.81	5.9-240	27±21
CGP116	0.6±0.1	45.41216	4.79475	230	100	13.071	6140	16.186	7603	7.627	4025	100	0.70	2.3-339	30±19
CGP117	0.15±0.05	45.31010	4.92852	217	100	3.389	1674	21.429	10584	7.673	4025	0	0.59	0.0-91.1	43±35
CGP119	0.15±0.05	45.33164	5.11978	319	100	1.514	850	18.370	10312	7.764	4025	0	0.46	0.0-32.9	33±20
CGP120	0.06±0.05	45.34966	5.57269	318	100	1.986	1206	21.129	12829	7.809	4025	0	0.55	0.0-98.6	38±23
CGP124	0±0	45.19684	5.75576	210	75	1.937	828	17.057	7290	7.946	4025	0	0.64	0.0-100	30±25
CGP125	0±0	45.18976	5.70102	210	100	2.108	1179	20.559	11497	7.990	4025	0	0.33	0.0-34.2	36±22

ρs (ρi) is the spontaneous (induced) track density (10^5 tracks/cm²); Ns (Ni) is the number of counted spontaneous (induced) tracks; ρd is the dosimeter track density (10^5 tracks/cm²); Nd is the number of tracks counted on the dosimeter; P(χ²) is the probability of obtaining Chi-square value (χ²) for n degree of freedom (where n is the number of crystals minus 1). Ages were calculated using the zeta calibration method [Hurford and Green, 1983], glass dosimeter IRMM540, and a zeta value of 255±8 yr/cm² calculated with Durango and Fish Canyon Tuff apatite standards.

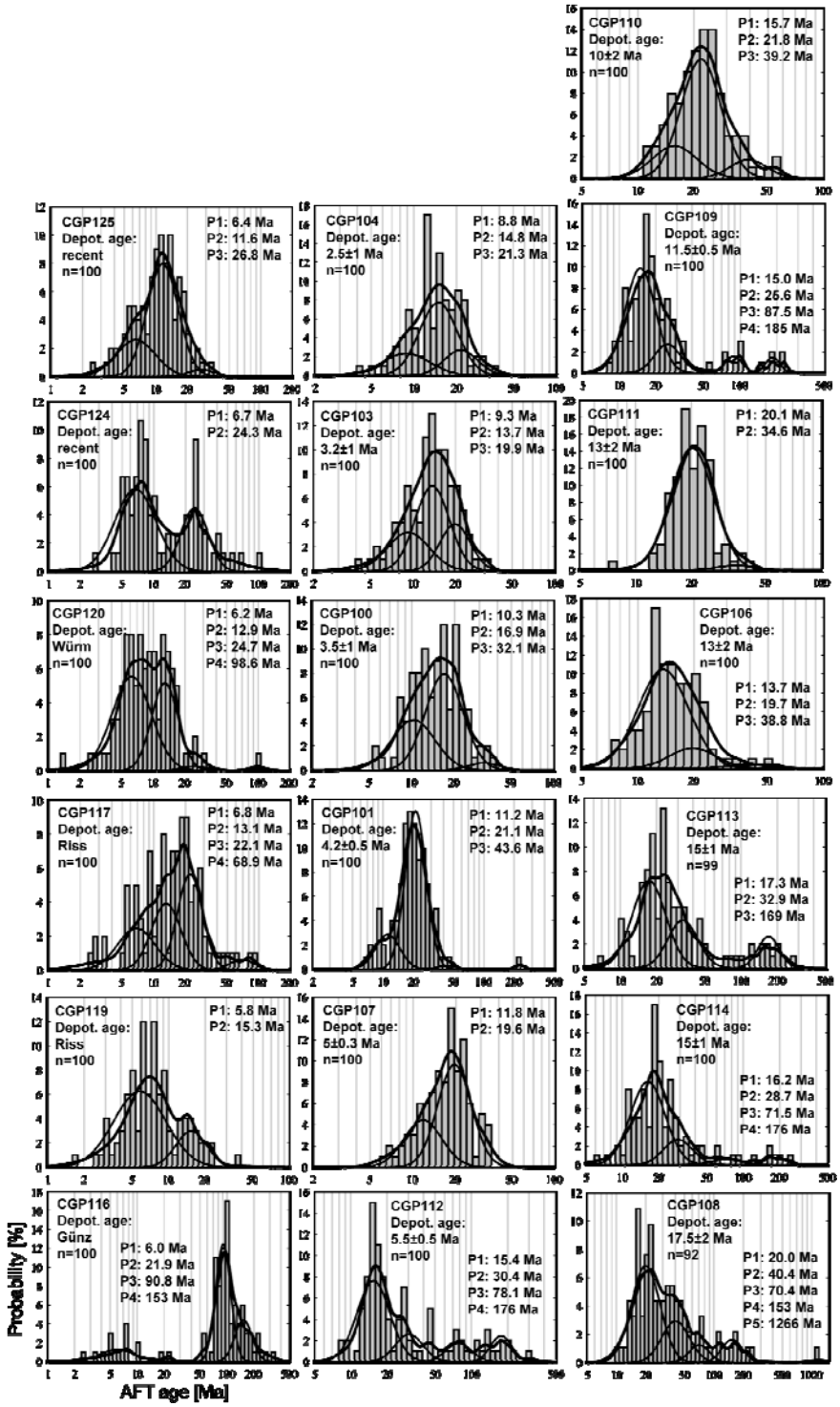

Figure DR1: Probability density plots of Miocene to present-day detrital apatite fission-track samples from the Chambaran basin. For each sample the depositional age, number of counted grains and fitted age-peaks are given. Binomial peak fitting was done with Binomfit program, described in Stewart and Brandon (2004) and Ehlers et al. (2005).

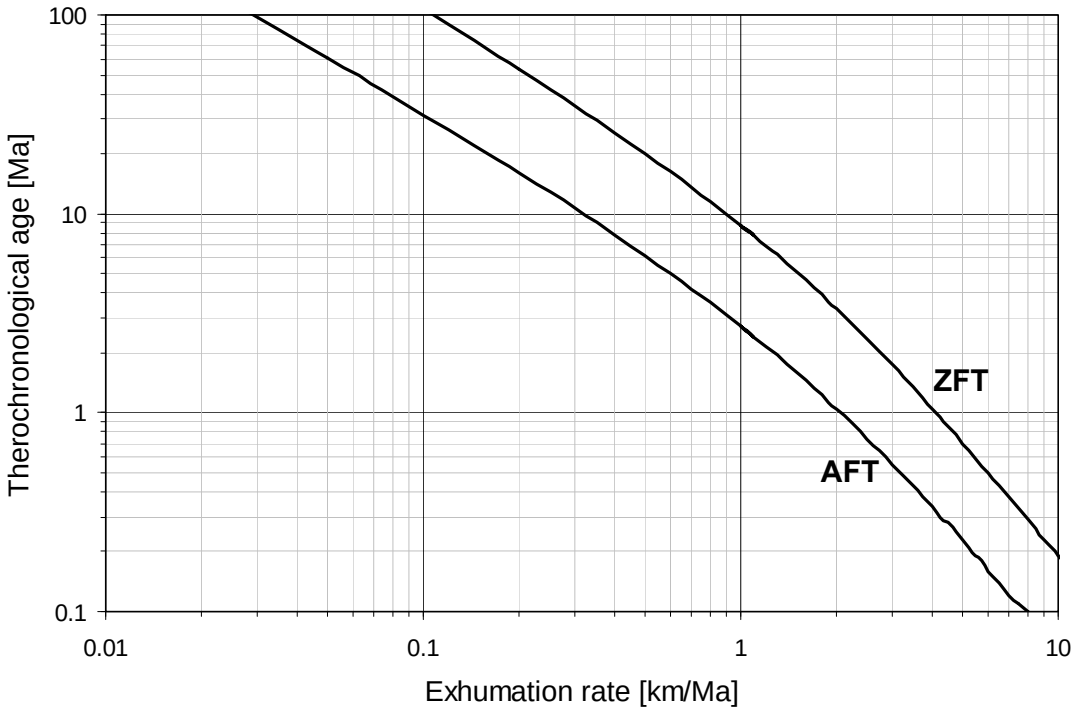

Figure DR2: Relationship between AFT and ZFT thermochronological ages and exhumation rates, calculated for a 1D steady-state thermal field using AGE2EDOT (Brandon et al., 1998). Thermal parameters are: model depth 30 km, thermal diffusivity 30 km²/Ma, heat production 8 °C/km, surface temperature 10 °C, surface thermal gradient for no erosion 30°C/km and annealing kinetics of Ketcham et al. (1999) and Tagami et al. (1998) for AFT and ZFT, respectively.

Appendix DR1: Depositional age of samples

Depositional ages are according to Clauzon et al. (1990, and references therein) and corresponding geological maps and explanatory notes published by the *Bureau de Recherches Gélogiques et Minières* (BRGM) (1:250,000: 29 Lyon; 1:50,000: 746 Vienne, 747 La Côte-St-André, 770 Serrières, 771 Beaurepaire, 794 Tournon, 795 Romans-S-Isère).

Sample CGP 108 is from Burdigalian marine sediments with an age of ~17.5 Ma (Clauzon et al., 1990) from a syncline within the Chartreuse Subalpine massif. Samples CGP 113 and 114 are from the "Sands of Clérieux", which have a Langhian age of ~15 Ma (Clauzon et al., 1990). Samples 106 and 111 are taken from Serravalian marine sands in the central Chambaran basin with an age of ~13 Ma. CGP 109 is from marine sands close to the marine/continental transition and has a Serravalian-Tortonian age of 11.5±0.5 Ma (Clauzon et al., 1990). Sample CGP 110 is taken from sand lenses in Tortonian conglomerates with an age of ~9 Ma.

CGP 107 is sampled from lower Pliocene marine deposits, which were deposited between the end of the Messinian salinity crisis at ~5.3 Ma (Krijgsman et al., 1999) and the marine/continental facies transition at ~4.7 Ma (Aguilar et al., 1989). At the same time clayey sediments were deposited close to Lens Lenstang. Sample CGP 101 is from well-sorted sands concordantly overlying these clays, suggesting a Pliocene age slightly younger than 4.7 Ma, probably ~4.2 Ma. Sample CGP 104 was taken a few meters below the strongly weathered abandonment surface sealing the Chambaran basin remnant, which has a minimum age of ~2 Ma as suggested by mammal fossils in overlying loess deposits (Guérin et al., 2004). Therefore we assume an age of ~2.5 Ma for sample CGP 104. Samples 100, 101 and 103 originate from a 'near-vertical' transect between sample 101 (~4.2±0.5 Ma at 330 m) and 104 (~2.5±1.0 Ma at 406 m). We interpolated the depositional ages for these samples according to their elevation, which should give a relative good approximation since rocks are only slightly tilted (<5°), show no discordance and consist of a single lithology (conglomerates with sand-lenses).

Samples CGP 116, 117-119 and 120 are from moraine deposits ascribed to pre-Mindel (~0.6 Ma), Riss (~0.15 Ma) and Würm (~0.05 Ma) glaciations, respectively (cf. BRGM 1:250,000 geological map of Lyon). Finally, CGP 124 and CGP 125 are from modern fluvial deposits of the Isère and Drac rivers, respectively.

Appendix DR2: Numerical modeling of detrital AFT ages

To verify the sensitivity of the presented detrital AFT dataset to predict exhumation histories, especially an increase in exhumation rates as suggested by the sediment budget (Kuhlemann, 2000), we produced theoretical AFT datasets and associated lag times for different exhumation scenarios comparable to previous approaches (e.g., Stock et al., 2006; Vermeesch, 2007; Whipp et al., 2009).
The model approach comprises three steps:

(1) The 3D thermal-kinematic code *Pecube* (Braun, 2003) is used to calculate theoretical surface AFT ages at each depositional age of samples, controlled by specified thermo-

kinematic and topographic input parameters (Table DR2), and using the AFT annealing model of Stephenson et al. (2006). Modeling was performed for the present-day topography of the Western Alps (the model extent is shown in Fig. 1a). Eight forward models were run, two models with a steady-state exhumation rate of 0.5 and 1.0 km/My and two times three models with a linear/stepwise increase in exhumation rate from 0.5 to 1.0 km/My since 5, 2.5 and 1 Ma, respectively.

(2) Predicted AFT datasets (1000 for each sample) were generated for each depositional age, taking into account the modeled surface AFT ages, number of counted grains of P1 and the Poisson-distributed measurement uncertainties (Vermeesch, 2007).

(3) Predicted AFT datasets all passed the Chi-square test at the 5% level, indicating a single age population. Therefore the central age of each predicted AFT dataset was used to produce predicted lag times (Fig. 4).

(4) Predicted AFT datasets (1000 for each sample) were generated for each depositional age, taking into account the modeled surface AFT ages, number of counted grains of P1 and the Poisson-distributed measurement uncertainties (Vermeesch, 2007).

(5) Predicted AFT datasets all passed the Chi-square test at the 5% level, indicating a single age population. Therefore the central age of each predicted AFT dataset was used to produce predicted lag times (Fig. 4).

Table DR2: Model input parameters		
Parameter	**Value**	**Unit**
longitude of lower left node	5.475788	°
latitude of lower left node	44.582176	°
cell size	0.008333	°
longitude cells	208	-
latitude cells	162	-
model thickness	35	km
T at base of model	700	°C
T at sea level	12	°C
atmospheric lapse rate	4.6	°C
heat production	0.6	µW/m³
thermal diffusivity	25	km²/Myr

Supplementary References

Aguilar, J.-P., Clauzon, G., Michaux, J., 1989, La limite Mio-Pliocène dans le Sud de la France d'apres les faunes de rongeurs; etat de la question et remarques sur les datations à l'aide de rongeurs, Bollettino della Societa Paleontologica Italiana, v. 28, p. 137-145.

Brandon, M.T., Roden-Tice, M.K., Garver, J.I., 1998, Late Cenozoic exhumation of the Cascadia accretionary wedge in the Olympic Mountains, northwest Washington State, Geological Society of American Bulletin, v. 110, p. 985-1009.

Braun, J., 2003, Pecube: a new finite-element code to solve the 3D heat transport equation including the effects of a time-varying, finite amplitude surface topography, Computers & Geosciences, v. 29, p. 787-794.

Clauzon, G., 1990, Genèse et évolution du piémont néogène subalpin du Bas-Dauphiné: Université d'Aix-Marseille II, Aix-en-Provence.

Ehlers, T.A., Chaudhri, T., Kumar, S., Fuller, C.S., Willett, S.D., Ketcham, R.A., Brandon, M.T., Belton, D.X., Kohn, B.P., Gleadow, A.J.W., Dunai, T.J., Fu, F.Q., 2005, Computational tools for low-temperature thermochronometer interpretation, in Reiners, P.W., Ehlers, T.A., eds., Low-Temperature Thermochronology: Reviews in Mineralogy and Geochemistry, v. 58, p. 205-238.

Guérin, C., Faure, M., Argant, A., Argant, J., Crégut-Bonnoure, É., Debard, É., Delson, E., Eisenmann, V., Hugueney, M., Limondin-Lozouet, N., Martín-Duárez, E., Mein, P., Mourer-Chauviré, C., Parenti, F., Pastre, J.-F., Sen, S., Valli, A., 2004, Le gisement pliocène supérieur de Saint-Vallier (Drôme, France) : synthèse biostratigraphique et paléoécologique, Geobios, v. 37, p. 349-360.

Ketcham, R.A., Donelick, R.A., Carlson, W.D., 1999, Variability of apatite fission-track annealing kinetics. III. Extrapolation to geological time scales, American Mineralogist, v. 84, p. 1235–55.

Krijgsman, W., Hilgen, F.J., Raffi, I., Sierro, F.J., Wilson, D.S., 1999, Chronology, causes and progression of the Messinian salinity crisis, Nature, v. 400, p. 652-655.

Kuhlemann, J., 2000, Postcollisional sediment budget of circum-Alpine basins (Central Europe), Memorie dell'Istituto di Geologia e Mineralogia dell'Universita di Padova, v. 52, p. 1-91.

Stephenson, J., Gallagher, K., Holmes, C.C., 2006, Low temperature thermochronology and strategies for multiple samples 2: Partition modelling for 2D/3D distributions with discontinuities, Earth and Planetary Science Letters, v. 241, p. 557-570.

Stewart, R.J., and Brandon, M.T., 2004, Detrital-zircon fission-track ages for the "Hoh Formation": Implications for late Cenozoic evolution of the Cascadia subduction wedge: Geological Society of America Bulletin, v. 116, p. 60-75.

Stock, G.M., Ehlers, T.A., Farley, K.A., 2006, Where does sediment come from? Quantifying catchment erosion with detrital apatite (U-Th)/He thermochronometry, Geology, v. 34, p. 725-728.

Tagami, T., Galbraith, R.F., Yamada, R., Laslett, G.M., 1998, Revised annealing kinetics of fission tracks in zircon and geological implications, *in* Van den haute, P.,De Corte, F., eds., Advances in fission-track geochronology: Kluwer academic publishers, Dordrecht, The Netherlands, p. 99-112.

Vermeesch, P., 2007, Quantitative geomorphology of the White Mountains (California) using detrital apatite fission track thermochronology, Journal of Geophysical Research, v. 112, doi:10.1029/2006JF000671.

Whipp, D.M., Ehlers, T.A., Braun, J., Spath, C.D., 2009, Effects of exhumation and topographic evolution on detrital thermochronometer data, Journal of Geophysical Research, v. 114, doi:10.1029/2008JF001195.